ISSN 0036-0244, Russian Journal of Physical Chemistry A, 2022, Vol. 96, No. 10, pp. 2222–2231. © Pleiades Publishing, Ltd., 2022.

PHYSICAL CHEMISTRY
OF SURFACE PHENOMENA

Physical Chemistry Study of Graphite Liquid Exfoliation through (π–π) Interaction by (*n*)-Annulene

Majid Monajjemi[a,c,*], Fatemeh Mollaamin[a], Narges Najaflou[b], and Hossein Sakhaeinia[c]

[a] *Department of Biomedical Engineering, Faculty of Engineering and Architecture, Kastamonu University, Kastamonu, Turkey*
[b] *Department of Chemistry, Science and Research Branch, Islamic Azad University, Tehran, Iran*
[c] *Department of Chemical Engineering, Central Tehran Branch, Islamic Azad University, Tehran, Iran*
** e-mail: m_monajjemi@srbiau.ac.ir*

Received August 23, 2021; revised August 30, 2021; accepted September 1, 2021

Abstract—π–π Non-covalent interaction, especially important in intermolecular interactions involving (*n*)-Annulene-graphene aromatic rings in particular, is fundamental for exfoliate processes. The work detailed in this study involves the application of electronic structure for illuminating of the (π–π) interactions between (*n*)-Annulene solvents and graphene sheets. We have simulated the adsorption of several (*n*)-Annulene and its Aza-bora derivatives on a graphene sheet, using QM/MM method with ONIOM approach. The presences of these compounds significantly alter the overall magnitude of exfoliation due to (π–π) interactions between Annulene solvents and graphene through rising of the strong interactions including π-orbitals of the adsorbent. Adsorption of individual molecules and Aza-bora compound reflects a hierarchical balance of the especial interaction that determines the overall energy of adsorption. In addition, the nucleus independent chemical shifts (NICS) and statistical nucleus chemical shifts (S-NICS) values confirm the amounts of aromaticity and anti-aromaticity in those rings.

Keywords: exfoliation, graphene, (*n*)-Annulene, (π–π) interaction, NICS

DOI: 10.1134/S0036024422100247

1. INTRODUCTION

1.1. Annulene Families

Annulenes belongs to a series of conjugated monocyclic hydrocarbons by formula C_nH_n (n = even) or C_nH_{n+1} (n = odd), such as (6)-Annulene (benzene), (4)-Annulene (cyclobutadiene), (8)-Annulene (cyclooctatetraene), and (14)-Annulene (cyclotetradecaheptaene) (Fig. 1).

Annulenes may be non-aromatic (10)-Annulene, or anti-aromatic (12)-Annulene, or aromatic (6)-Annulene. Cyclooctatetraene (COT) or (8)-Annulene which is a poster child for non-aromatic molecules was first synthesized by Richard Willstatter [1]. Coupling between COT^{2-} charges states and their mechanical conformations construct a new position for COT^{2-} as an aromatic molecule including electromechanical converter treatment. Planar conjugated

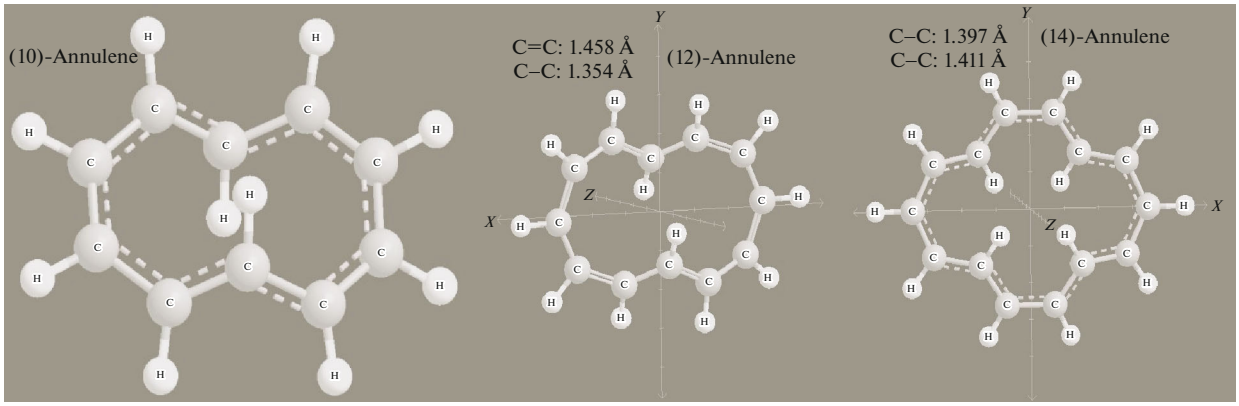

Fig. 1. Geometries optimized of variants of (*n*)-Annulene (n = 10, 12, and 14).

COT^{2-} exhibit a powerful link between π-electrons in its molecular structure. Huckel's "$4n + 2$" rule indicates a mono aromatic ring from anti-aromatics with their magnetic properties. Although COT that follows a non-planar conformation with alternating double and single bonds via D_2d symmetry is not an aromatic molecule, $C_8H_8^{2-}$ di-anion "Cyclooctatetra-enide" is an aromatic ion with suitable resonance energy. This di-anion is planar and octagonal in its structure and aromatic with the Huckel electron count of 10. Through the interaction between alternating bonds it has been confirmed that the structures of COT undergo a thermal shift bonding and ring inversion operations including a planar transition state of D_{4h} [2–7]. In addition the NMR data indicate that COT's di-anion (COT^{2-}) adopts with a D_{8h} symmetry structure. Although the planar D_{4h} structure for the ring inversion of COT has a transition state (TS) with barrier energy around 12 kcal mol^{-1} [8–10], the D_{8h} bond switching TS lays a few kilo calories per mole higher. Actually, COT has three fundamental structural changing including 1: ring inversions, 2: bond shifts, and 3: valences isomerization [11–14].

These conformational structures help increase the efficiency of graphite to graphene exfoliation due to ring inversion and shifting phenomenon.

Steiner and Fowler investigated a model via frontier-orbital contributions which yields an accurate result of π ring currents in benzene, COT^{2-} and such other planar rings [15]. London [16], Pauling [17], and Pople [18] investigated the concept of aromaticity and anti-aromaticity in viewpoint of magnetic criterion, diatropic (planar of $4n + 2$ systems) and paratropic currents (planar of $4n$ systems). In recent decades it has been exhibited that the ring current is an outcome of the HOMO–LUMO transition depends on symmetry properties and current-densities localized circulations around the electronegative nucleus [19]. Interactions among aromatic π systems are one of the major non-covalent interactions controlling macro molecular systems and these aromatic π–aromatic π interactions are present in diverse range of research especially in molecular engineering and nano-modeling. Unlike well-researched hydrogen bond interactions, the π–π interaction is difficult to model due to the unknown intermolecular mechanism. So, the electronic structures, dispersion, NBO analysis, NMR investigation, induced currents in aromatic-rings, have main role in stabilizing these interactions between graphite and Annulene in exfoliation.

1.2. Liquid-Phase Exfoliation (LPE)

A certain way for producing graphene is a liquid-phase exfoliation (LPE) method. Graphite can be exfoliated in solvents such as benzene or (6)-Annulene, cyclooctatetraene (8)-Annulene and cyclotetradecaheptaene (14)-Annulene to extract individual layers. For exfoliation, prevailing the van der Waals forces between the neighbor layers of graphite is an essential factor [20–23]. Liquid plunging is the most important technology for reducing the strength of the van der Waals forces between two graphite layers. The potential energies among the layers are given by the dispersive London interactions, which are extremely decreased with respect to vacuum by the attendance of a solvent. The situation of graphene and liquid surface energies is one main factor for a successful LPE mechanism. Coleman exhibited that the major factor for appropriate solvents is that the solvent-graphene forces might be at least similar to the stacked graphene. Therefore, suitable liquids are defined based on liquid's surfaces tension in the range of around 35–55 mJ/m^2 [23–25]. By this work, It has been exhibited that the aromaticity-aromaticity (π–π) interaction with graphene is much more stronger than the van der Waals forces between two graphite layers in graphene due to induced currents between aromatic-rings which produce attractive forces in one side and in the opposite side make the repulsive forces (Fig. 2). Two kinds of bond appear among the graphene layers, one bond that keeps together the layers by the weak through Vander Waal force (the neighbor layers around 3.40 Å). Because of these weak forces between two layers, the sheets slide each other and therefore the aromaticity-aromaticity (π–π) interaction is strong enough to do the exfoliation. The second bond is a strong Covalent bond which exists between the carbon-carbon atoms in each layer (1.41 Å). The LPE mechanism generally includes three steps; dissolve graphite in liquids media, exfoliation and purification. Loh et al. [26], exhibited the exfoliation is better when the surfaces energies of the solvents are near to the graphene. Obviously through the mechanical forces which are greater than Vander Waals interaction the graphene layers can be separated completely.

1.3. Thermodynamic of Exfoliation of Graphene in Solvent

Thermodynamic study is a strong tool for investigating the popularization, dispersion and exfoliation of graphite in solvents. Based on a thermodynamic model [27, 28], enthalpy of mixing of graphite per volume of solvent can be written as follows.

$$\frac{\Delta H_{\text{mix}}}{V} \approx 4\left(\sqrt{E_{\text{s,G}}} - \sqrt{E_{\text{s,sol}}}\right)^2 \frac{\varnothing}{D}, \quad (1)$$

where ∅ indicates the dispersion of graphite volume fraction and D is the dispersed thickness. In addition $E_{\text{s,sol}}$ and $E_{\text{s,G}}$ are solvent and graphite surface energies, respectively. Therefore, based on the role of surface energies, it might be a successful approach for exfoliating graphite to give graphene in the certain solvents. We initially focused on several known solvents which applied to exfoliate graphite such as Pyrene

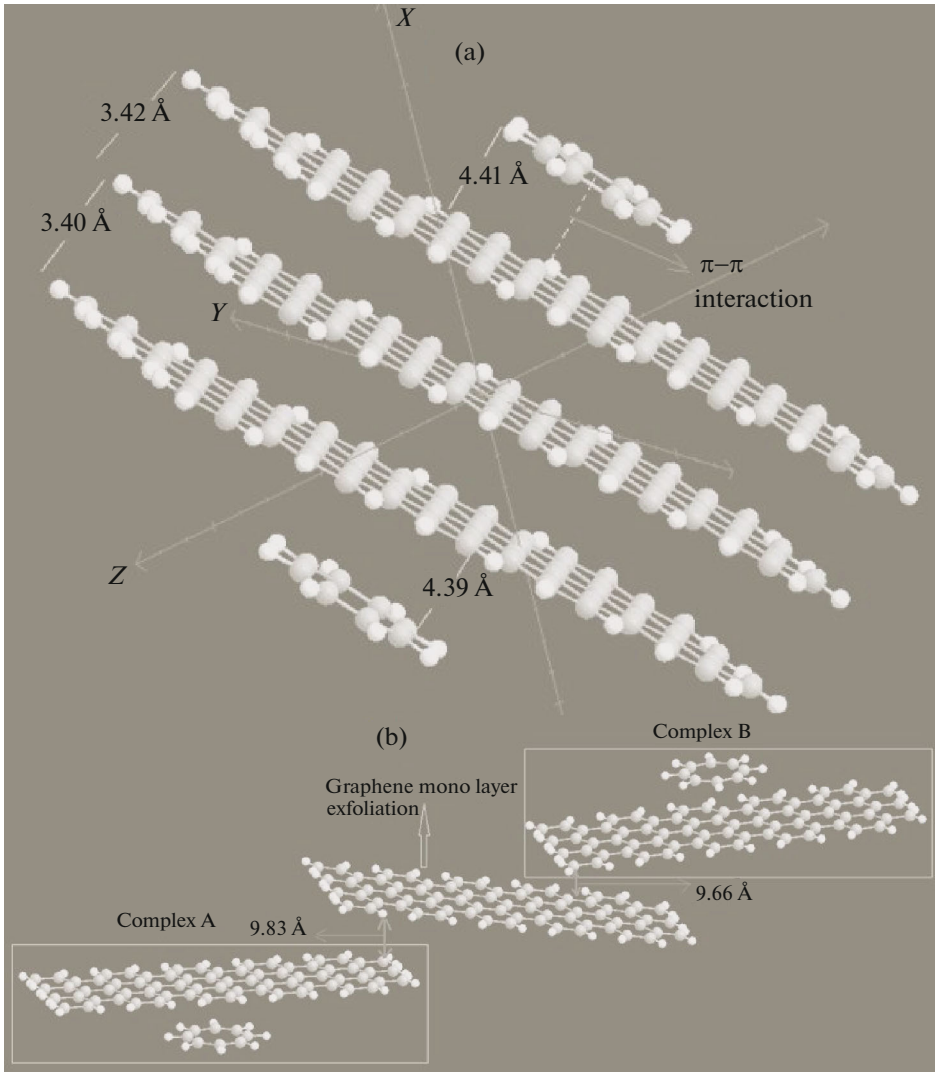

Fig. 2. (a) Optimized molecule including 3 layer graphene and two molecules of (8)-Annulene $C_8H_8^{(2-)}$ with ONIOM methods including two levels of, high-medium basis sets, (b) optimized molecule including middle step of graphite exfoliation with (8)-Annulene.

derivatives. Since the distances among stacked parallel layers of graphene in graphite are around 3.4 Å, any planer molecules with thicknesses less than this amount might be suitable for exfoliating. Although the van der Waals attraction between two neighbor layers is loose, the attraction is a little bit strong for making exfoliation into individual layers challenging. A prosperous exfoliation needs the overbearing of the van der Waals forces among several layers at once. One of the most effective ways to reduction the strength of the van der Waals attraction is liquid immersion, where the potential energies among those layers are contributed through the dispersive London interactions. Therefore, the interfacial tension plays a key role when a solid surface is plunge in a liquid medium. Due to the high interfacial tension in graphite layers and tending to cohere to each other, the cohesion between them is high and also impediment their dispersion in the liquids. Generally, water has the most advantage for the solid surface energy, due to surface tension (21.8 mJ/m^2 with the polar phase of 51.0 (mJ/m^2). (*n*)-Annulene family with high surface tension is suitable solvent for the dispersion of graphitic flakes in view point of thermodynamic phenomenon (Fig. 3). By this work we calculated the enthalpy mixing ΔH_{Mix} of graphene flakes dispersed in solvents via equations as follow:

$$\frac{\Delta H_{\text{Mix}}}{V} \approx \frac{2}{T_{\text{NS}}}(\sqrt{E_{\text{s,s}}} - \sqrt{E_{\text{s,G}}})^2 \varnothing_{\text{G}}, \qquad (2)$$

where $E_{\text{s,G}}$ and $E_{\text{s,s}}$ are the graphene and (*n*)-Annulene family solvents surfaces energies, respectively.

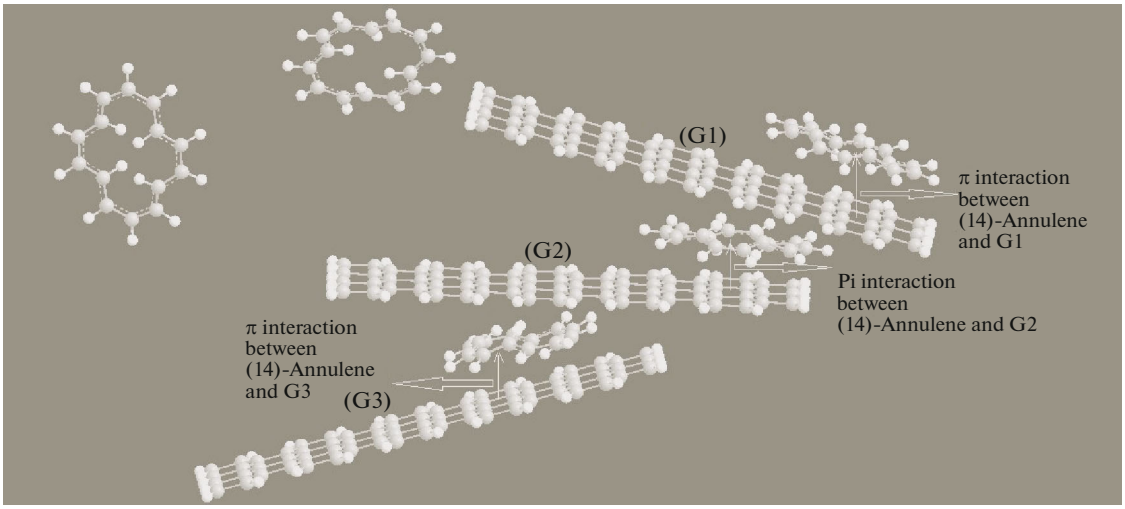

Fig. 3. The position of one side π interactions between graphene sheets and (14)-Annulene.

T_{NS} is the thickness of nano sheet while $\varnothing_G$ is volume fraction of graphene dispersed which are related to the diameter of graphene sheet D_G and concentration of graphene C_G as follows:

$$C_G \propto \exp\left(-\frac{\pi D_G^2}{8E_{s,G}KT}\right)(E_{s,s} - E_{s,G}). \quad (3)$$

We find exact data around ~65 mJ/m^2 close to the work of contact angle measurements [29].

1.4. π–π Interactions

Interactions between aromatic π systems of graphene sheet to other planer molecules such as (*n*)-Annulene are one of the major non-covalent forces governing exfoliation processes. In fact the importance of π–π interactions is widely known among chemists with their energies around 2–3 kcal mol^{-1}. This small value causes a challenge for both theorists and experimentalists for obtaining an obvious meaning of their roots. In contrast to hydrogen bonds, π–π interactions are difficult for any modeling due to the several centers of intermolecular contact. Characterization of π–π interactions experimentally has difficulties, but computational studies can be exhibited important information in solvents. A number of experimental and theoretical studies have been applied benzene dimer as a prototype of the π–π stacking interactions [30].

We focused in the electrostatic, dispersion, exchange repulsion and induction forces which all play a major role in the interaction between graphene rings and (*n*)-Annulene solvents. The priority of this investigation is calculation of prototype binding energies of aromatic π–π interactions between graphene with (*n*)-Annulene which have been simulated using highly large basis sets and methods. Results from this work predict the parallel-displaced configurations of graphene-(*n*)-Annulene solvents are the best position for exfoliation. π–π stacking interactions can be interpreted based on polarization effect that electron-withdrawing substituents enhance. π–π stacking interactions through reduction of electrostatic repulsion among π clouds of the rings, but electron-donating ones prevent those interactions.

Sinnokrot [31] exhibited that electron donating, reclaim strength of the π–π systems. Wheeler shown, the substituent effect in benzene dimers depends to the electrostatic interactions among the substituents on one ring and the un-substituted on opposite ring [32]. Ringer and Steven Wheeler exhibited the dispersion effects for explaining the reason of these substituted stacked of complexes and also Local nature of substituent effects in the π–π interactions [32, 33]. In some works, it has been discussed that anti-aromaticity of the 4*n*–π electrons of the hydrocarbon rings can eliminate through π–π stacking interactions [34]. In other words, π–π interactions are the way for achieving aromatic rings with 4*n*–π electrons and also the effect of π–π stacking with more π-electron rings propel to a super aromaticity which can be interpreted as stacked-ring aromaticity in organic compounds [35]. In this study, concurrent effects of various (*n*)-Annulene with considering anti-aromaticity or aromaticity on the strength of π–π stacking interactions have been estimated in Annulene–Graphene complexes direct electrostatic interactions between one ring and π electron cloud of the other ring usually impact on the π–π stacking interactions. For investigating well-mannered effects of the π–π stacking interactions, various (*n*)-Annulene including $n = 8$, 10, 12, 14, and 16 have been selected and simulated (Fig. 3).

2. THEORETICAL AND EXPERIMENTAL BACKGROUND

2.1. Isotropic and Anisotropic Parameter

Total chemical shift tensors σ are a non-symmetrical tensors which can be separated through three independent parameters which are known as isotropic, traceless symmetric, and traceless anti-symmetric. In addition, a spherical tensor has been exhibited by Haeberlen [36], Mehring [37], and Diehl [38]. They have investigated fundamental tensors as

$$\sigma = \sigma^{iso(0)} + \sigma^{anti(1)} + \sigma^{sym(2)}. \quad (4)$$

Spherical tensors can also be written as

$$\sigma_0^{iso(2)} = \sqrt[2]{3/2}\delta_{(zz)} \quad \text{and} \quad \sigma_{\pm 2}^{sym(2)} = \frac{1}{2}\delta_{(zz)}, \quad (5)$$

where $\delta_{(zz)}$ is the reduced anisotropy and can be calculated through

$$[\delta_{(zz)} = (\sigma_{zz} - \sigma_{iso}) = (\sigma_{33} - \sigma_{iso})]. \quad (6)$$

This parameter is related to the anisotropy ($\Delta\sigma$) with

$$\Delta\sigma = \frac{3}{2}\delta_{(zz)}. \quad (7)$$

From Eqs. (7) and (8) asymmetry (η) shielding can be estimated as:

$$\Delta\sigma = \sigma_{zz} - \frac{1}{2}(\sigma_{xx} + \sigma_{yy}), \quad (8)$$

$$\eta = \left(\frac{\sigma_{yy} - \sigma_{xx}}{\delta_{(zz)}}\right) = \frac{3(\sigma_{yy} - \sigma_{xx})}{2\Delta\sigma} \text{ [39]}. \quad (9)$$

The magnetic resonance of the spins are seldom isotropic, therefore they must represent with new tensors (Herzfeld-Berger notation) [40]. These tensors are known as Span (Ω) $\Omega \geq 0$, which illustrates the maximum width of the model and the skew (κ) of the tensors which are a magnitude of the values

$$(\Omega) = \sigma_{33} - \sigma_{11} \quad \text{and} \quad \varkappa = \frac{3(\sigma_{iso} - \sigma_{22})}{\Omega}. \quad (10)$$

Moreover the orientation of skew (κ) is given by

$$\varkappa = \frac{3(\sigma_{iso} - \sigma_{22})}{\Omega} \quad (-1 \leq \kappa \leq +1). \quad (11)$$

In some items of an axially symmetric tensors ($\sigma_{yy} - \sigma_{xx}$), might be zero and therefore $\eta = 0$. In addition, the asymmetry (η) indicates where how much deviation can be appeared from the axially symmetrical tensors, so the region of η is between zero and one ($0 \leq \eta \leq +1$).

NICS is a simple method by Schleyer and coworkers which estimates the absolute magnetic shielding in the center of molecules, minus NICS amount indicates aromaticity and positive result indicates antiaromaticity [19].

2.2. Current Electron Density, ELF, and LOL Functions

The current densities can be rearranged as:

$$\rho(r) = \eta_i |\varphi_i(r)|^2 = \sum_i \eta_i \left|\sum_l C_{l,i}\chi_i(r)\right|^2. \quad (12)$$

That χ is the basis function of orbitals and η_i is occupation number. *C* is also a coefficient matrix. Bader [41] illustrated, regions of large electron localization have a wide value of Fermi-hole. Becke and coworkers [42] illustrated that spherically average like-spin pair has suitable correlation with the Fermi hole. Consequently, they introduced a new function as electrons localization functions (ELF)

$$\text{ELF}(r) = \frac{1}{1 + [D(r)/D_{0(r)}]^2}, \quad (13)$$

where

$$D(r) = \frac{1}{2}\sum_i \eta_i |\nabla\varphi_i|^2 - \frac{1}{8}\left[\frac{|\nabla\rho_\alpha|^2}{\rho_\alpha(r)} + \frac{|\nabla\rho_\beta|^2}{\beta(r)}\right] \quad (14)$$

and

$$D_{0(r)} = \frac{3}{10}(6\pi^2)^{2/3}[\rho_\alpha(r)^{5/3} + \rho_\beta(r)r)^{5/3}] \quad (15)$$

for closed-shell systems, since $\rho_\alpha(r) = \rho_\beta(r) = \frac{1}{2}\rho$, *D* and D_0 terms can be simplified as

$$D(r) = \frac{1}{2}\sum_i \eta_i |\nabla\varphi_i|^2 - \frac{1}{8}\left[\frac{|\nabla\rho|^2}{\rho(r)}\right] \quad (16)$$

and

$$D_{0(r)} = \frac{3}{10}(3\pi^2)^{2/3}\rho(r)^{5/3}. \quad (17)$$

Savin et al. [43], indicated which $D(r)$ determines the excess kinetic energies due to the Pauli repulsion, while $D_0(r)$ is known as Thomas–Fermi kinetic energies term. In other words they re-considered the ELF in view point of kinetic energy through Kohn-Sham DFT's wave-function. Therefore ELF would be in the range of [0, 1] and a large ELF value indicates that electrons are strongly localized. ELF is used for the wide varieties of molecules, such as organic, inorganic, atomic crystals, coordination compounds, clusters, and also for aromatic rings. Localized orbital locator (LOL) is the other function similar ELF that has been investigated by Becke and coworkers [44]

$$LOL(r) = \frac{\tau(r)}{1 + \tau(r)}, \quad \text{where} \quad (r) = \frac{D_0(r)}{\frac{1}{2}\sum_i \eta_i |\nabla\varphi_i|^2}, \quad (18)$$

$D_0(r)$ for both spin-polarized and closed-shell systems are explained in the same meaning as in ELF. Jacobsen exhibited that LOL supply more definitive and obvious image than ELF, therefore LOL can be inter-

Table 1. Average straight-line distances traveled by a graphene on a graphitic layers, experimental flake has been estimated by Feng et al. [48]

Simulation		
temperature of simulation	graphite layers distances, nm	suspended graphene
10	55.5	49.5
100	52.5	39.5
200	50.5	35.5
300	49.2	33.1

Experimental [48]	
temperature	distances, nm
5	95
77	35

preted in kinetic energies way better than ELF; as regards LOL can also be interpreted in viewpoint of localized orbital. The value ranges of LOL are similar to ELF between zero and one [0, 1].

3. COMPUTATIONAL DETAILS AND RESULTS

Each part of the systems including (*n*)-annulene and solvents have been optimized using ab initio with DFT calculations individually. Whole of the graphite layers including (2)–(10) graphene layers and with π–π stacking interactions among those layers and (*n*)-annulene have been calculated with QM/MM methods through an ONIOM approach. In our study, differences of force fields are debated through comparing density and energies with OPLS and AMBER via Monte Carlo calculations. In addition, a Hyper-Chem professional release 7.01 program has been applied for some additional keywords such as PM3MM, PM6 (pseudo=lanl2).

The final parameterization of exfoliation in order to find the optimal starting geometries, as well as the difference energies for those structures (Figs. 2, 3) were accomplished through the equation

$$\Delta E_i \text{ (eV)} = \{E_{\text{sys}} - (E_{\text{nG}} + E_{[n]\text{annulene}} + E_{\text{solvent}}\} + E_{\text{BSSE}}. \quad (19)$$

Van der Waals densities functional with the DFT was investigated for modeling of exchange-correlation estimation. All optimizations of graphene layers were done by Gaussian-09 [8]. The accurate calculations performed using m062x, m06-L, and m06 for *cis*–*trans* conformations. The m062x, m06-L, and m06-HF methods have a suitable correspondence in non-bonded calculations between two graphene and (*n*)-Annulene. The ONIOM levels have been applied through 3 levels of high (H), medium (M), and low (L) calculations which DFT methods were used for the high (H) layer and the semi empirical method of pm6 and Pm3MM was used for the medium and finally Monte Carlo for low layers, respectively. The surface adsorption energies among various situations of (*n*)-Annulene were calculated according to the equation:

$$\Delta E_{\text{adsorption}} \text{ (eV)} = \{E_{\text{graphite}} - nE_{\text{graphene}} \ (n = 2\text{–}10) + E_{[\text{annulene}]}\} + E_{\text{BSSE}}. \quad (20)$$

Several physical properties such as electron densities, values of orbital wave-functions, electron spin densities, electron localization function (ELF), localized orbital locator (LOL defined by Becke and Tsirelson), total electrostatic potential (ESP), as well as the exchange-correlation densities, and the average local ionization energies using the Multifunctional Wavefunction analyzer have been also calculated and are listed and discussed in proper sections. Calculations of electronic structure were based on model of graphene sheet containing 400 carbon atoms with optimized C–C and C–H bond distances 1.46 and 1.01 Å, respectively.

4. DISCUSSION

Using classical molecular dynamics simulations with OPLS, BIO+, MM+, and Amber force fields (see the Computational Methods), have been done for the complex system of the (graphene–graphene), (graphene–Annulene), and (graphene–Annulene–solvents). These force fields apply especial non-bonded potentials via various data from experiments and quantum calculations [45–47]. The energies barrier for graphene sheets sliding allows us to model the behavior of motion of the graphene slides between 8–12 nm in diameter. Due to the anarchic nature of the graphene motion over the layers, a large number of simulations were performed, from which we analyzed the average distances (Table 1) [48–52].

Obviously, the standard force fields including Lenard–Jones non-bonded interactions are not useful for these types of simulations, therefore the motion of a graphene over the graphitic layers' substrate is characterized through fleeting alignments with the underlying lattice during which the energies are converted between translational and rotational energy.

We simulated and measured the surface energies of single-layer graphene–Annulene based on Eqs. (1)–(3) in several solvent media in viewpoint of the magnitude of π–π repulsion and strengthening adsorption (Table 2). The system for π–π interaction exhibits the decreased densities of π-electrons on an aromatic ring due to π–π repulsion between the ring and graphene layers, thereby leading to stronger adsorption. In fact, however, the adsorption of (12)-Annulene is weaker than the (10)-Annulene due to the decreasing of the π–σ attractions. We conclude that the presence of electron-withdrawing substituents on (*n*)-Annulene reduces both repulsive (π–π) and attractive (π–σ)

interactions between the aromatic core and graphene (Fig. 4).

This predicts that the adsorption of (*n*)-Annulene on graphite is driven primarily by medium-range interactions through long-range π–π interactions between the surface and the aromatic core of theme. Based on Eqs. (4)–(11), as it can be seen in Tables 3, 4, the NICS value for (12)-Annulene is smaller than the (10)-Annulene therefore the exfoliation of graphite towards graphene is a function of aromaticity due to π–π repulsion and these sequences are as follows: (14)-Annulene > (10)-Annulene > (12)-Annulene > (8)-Annulene.

Based on Eqs. (4)–(11) and the Herzfeld–Berger and Haeberlen convention of NMR components (Table 3), the NICS and S-NICS values can be determined for estimation the aromaticity and anti-aromaticity. In the long-range, π–π interactions between the surface of graphene and the (*n*)-Annulene core (also its Aza-bora derivatives) are important factor for exfoliation process of graphite towards graphene. As described, the attractive medium ranges interaction result primarily from a charge-transfer process caused by exchange and correlation (XC) effects among those aromatic rings and the graphene surface, rather than from an ensemble of electrostatic multiple interactions. The deviation in Fig. 4 is due to the π–π repulsion of the (*n*)-Annulene and also its Aza-bora derivatives interacted with graphene surface. It should be mentioned that benzene can be located on the surface of graphene with a parallel situation whose structure is positioned around 3.20 Å above the surface while for (*n*)-Annulene and their Aza-bora derivatives the geometry of adsorbed variant is significantly different.

The aromatic core is now tilted directed toward the surface. The significant attractive interaction between the Aza-bora and graphene brings larger to the surface than observed in the case of benzene. With decreasing the distances between the adsorbate molecules and graphene the π–π repulsion will be increased. Moreover, tilting of the ring follows exactly the asymmetry induced current via binding of aromatic ring underlying surface, where the π–π distance between (*n*)-Annulene and graphene is shorter than the one between benzene and graphene.

The effects of induced current attractive and repulsive π–π interactions become clear in the case of Aza-bora derivatives of Annulene adsorbed on surface, due to the stabilizing and strong interactions of BN bonds, but it becomes deformed for minimizing π–π repulsion.

The deformations involve bending the substituents out of the average plane of the aromatic core, allowing them to approach the surface without simultaneously bringing the core and the surface into closer contact. We have extended our theoretical methods on exfoliation by examining the effect of the very strongly electron-attracting B and N atoms, which is expected to minimize repulsion and attractive π–π interactions. As shown in Table 2, the energy of adsorption of Aza-bora compounds (NB) is larger than the one of (*n*)-Annulene. Based on energies magnitudes of adsorption and π–π repulsion the intensity of exfoliation might be evaluated for any further liquids and solvents. For better understanding, the nature of the (*n*)-Annulene–graphene interaction and also strong exfoliation, based on Eqs. (12)–(18) the electronic properties of the adsorbed states such as ELF, LOL, and HOMO/LUMO gaps have been studied. The highest occupied molecular orbital (HOMO) and lowest unoccupied molecular orbital (LUMO) of compounds are listed in Table 4. The HOMO is mostly localized on oxygen atoms and corresponds to low energies lone pairs of nitrogen. In contrast, the LUMO is delocalized over the entire molecule, but the shape of the contours reveals contributions from the π*-orbital associated with the benzene ring. ELF current-density map from ab initio calculations of (*n*)-Annulene and its Aza-bora derivatives are shown in (Fig. 5) and the currents are dominated by HOMO contributions (Table 5). In a ring with "4*n* + 2" system, the HOMO–LUMO are related to "*n* + 1" and "*n*," but for a ring with "4*n*" electrons, they are derived

Table 2. Energy of adsorption of substituted derivatives of benzene on graphene

Molecules	Adsorption energies, eV	π–π repulsion, kcal/mol
(8)-Annulene	0.214	2.55
(12)-Annulene	0.298	3.85
(10)-Annulene	0.312	4.99
(14)-Annulene	0.355	6.12
(14)-B7N7H14 Annulene	0.534	5.12
$B_4N_4H_8^{2-}$	0.443	4.98
C_6H_6	0.201	2.88

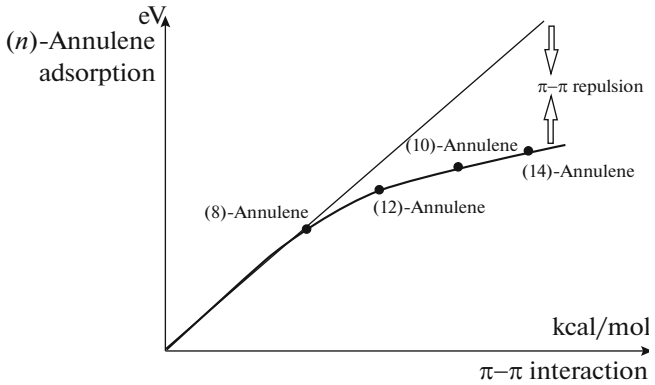

Fig. 4. The calculated adsorption energy for (*n*)-Annulene over a single carbon atom of the surface.

Table 3. Herzfeld-Berger and Haeberlen convention of NMR components with Cam-b3lyp/cc-pvdz of (*n*)-Annulene (*n* = 8, 10, 12, and 14) and its Aza-bora derivatives in various methods compare to benzene

Molecule	σ_{11}	σ_{22}	σ_{33}	σ_{iso}	$\Delta\delta$	κ	Ω	η	NICS	S-NICS
(10)-Annulene	−4.81	14.54	23.0	10.91	27.93	0.39	27.81	0.53	−10.91	−10.83
(12)-Annulene	−27.8	−0.93	16.30	−4.15	−35.5	0.22	44.12	0.72	4.15	4.11
(14)-B7N7H14 Annulene	−9.57	4.31	4.96	−0.09	−14.2	0.91	14.53	0.06	0.09	0.00
(14)-Annulene	2.97	3.97	37.92	14.95	34.45	−0.94	34.95	0.05	−14.95	−14.66
Benzene C_6H_6	5.55	6.28	13.86	8.56	7.94	−0.82	8.30	0.14	−8.56	−8.61
$C_8H_8^{2-}$	3.4	3.4	40.9	15.9	37.6	−0.99	33.7	0.0	−15.9	−15.82
$B_4N_4H_8^{2-}$	1.97	1.97	23.57	9.17	21.6	−0.99	21.6	0.0	−9.17	−8.25

Table 4. Geometry and energy of (*n*)-Annulene (*n* = 8, 10, 12 and 14) and its Aza-bora derivatives in various methods

Methods	Energy, Hartree	Relative stabilities energies, kcal/mol	X–X and X–H X = (C, B, N) in ring, Å		X–X–X and H–X–X angles X = (C, B, N)	LUMO/HOMO Gap, kJ mol^{-1}	Aromaticity	
							NICS	S-NICS
(10)-Annulene								
CAM-b3lyp/6-31g*	−386.9664044	−49259.9	X–X; C–C	1.368	CCC = 129.1	350.24	−10.91	−10.83
			X–X; C=C	1.422	CCC = 121.9			
			X–H; C–H	1.08	CCH = 113.3			
$B_4N_4H_8^{2-}$								
Cam-b3lyp/cc-pvtz	−323.1235597	−9197.97	X–X; B–N	1.445	BNB = 142.6	434.94	−9.17	−8.25
			X–H; B–H	1.243	NBN = 127.4			
			X–H; N–H	1.015	HBN = 116.3			
					HNB = 108.7			
(12)-Annulene								
Cam-b3lyp/6-31g*	−464.3714106	−97832.37	X–X; C–C	1.368	CCC = 129.1	260.41	4.15	4.11
			X–X; C=C	1.448	CCC = 122.2			
			X–H; C–H	1.09	HCC = 115.7			
					CCH = 113.3			

from a split degenerate ($\lambda = n$). For $n = 4$, λ is zero meanwhile dia-tropic contribution occurs from a transition in which $\Delta\lambda = +1$ and a para-tropic contribution occurs from a transition in which $\Delta\lambda = 0$ [14, 15]. In Huckel theory for *N* atoms with equal coulomb parameters $\{\alpha\}$ and equal resonance parameter $\{\beta\}$, the $\{\pi\}$ energies can be calculated easily by the well-known method [53]. Therefore, for the $4n + 2$ systems (with higher symmetry) only the HOMO–LUMO transitions (dia-tropic current) and for the "$4n$" ring (lower symmetry) two forms can be considered; first the HOMO–LUMO transition leads to a para-tropic contribution, and second HOMO–LUMO+1 transition to the dia-tropic contributions.

The lonely occupied-virtual-translational (OVT) transition in the $4n + 2$ system are therefore HOMO to LUMO, and so, in this system of a mono-ring, the ring current occurs only from the HOMO orbitals which are fully diamagnetic, but in $n = 0$ the HOMO with degeneracy = 2 and the $4n + 2$ system has four-electron in diamagnetism situation. In $4n$, the $\{\pi\}$ systems have half-filling of the angular momentums, therefore in full D_{nh} symmetry; it goes towards to an open-shell configuration with a distorting degeneracy. By reducing the symmetry HOMO and LUMO pairs split into non-degenerate orbitals relevant via a rotational transition with the small energies divisors. As it can be seen in Table 5, the gap energies, HOMO/LUMO overlap amounts and HOMO/HOMO–1 overlap amounts in whole spaces obey such of the sequences which can be considered as (1) HOMO/LUMO overlap amounts as an index for aromaticity (2) HOMO/HOMO–1 overlapping as index for anti-aromaticity. These HOMO/LUMO overlapping indicate the sum over states, producing a strong two-electron paramagnetic ring current. Other

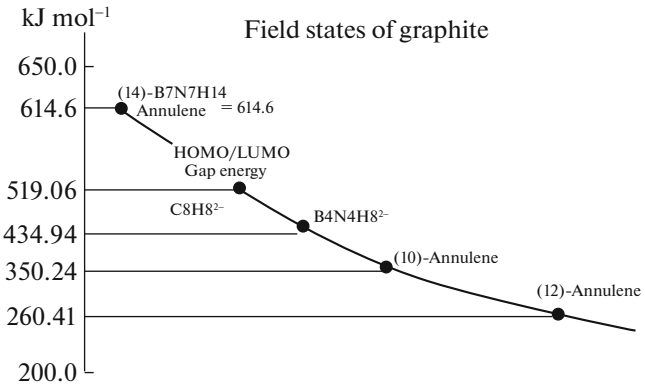

Fig. 5. Variation in the energy of the formal HOMO/LUMOs and the degree of charge transfer from graphene to various Annulene versus π–π repulsion.

rotational and translational transition is presented through the lowering in symmetry and actually has a minor important in small cycles.

CONCLUSIONS

(1) We conclude that the amounts of medium-range interactions are straightly dependent on the capacities of the adsorption to accommodate additional charges from the graphene sheets. For molecules such as Annulene with a low electron affinity, the strong binding for any further graphite exfoliation is determined through long-range π–π interactions.

(2) We have exhibited the presence of electronegative atoms such as nitrogen and boron can significantly alter the nature and the magnitude of interactions between small aromatic molecules and graphene towards strong exfoliation of graphite.

(3) During the substituents can simultaneously permit the formation of covalent bonds between B and N adsorbed atoms, it is possible for evaluating the relative contributions of percent the composition of atoms for HOMO/LUMO and HOMO/LUMO overlapping in whole space due to π-based interactions (Table 5).

(4) Three kinds of interactions support the explanation and determination of the nature in the ultimate structure for any further exfoliation including first: long-range repulsive π–π interactions between 2 to 7 kcal mol^{-1} (Table 2); second: medium-range attractive π–π* interactions between 6 to 12 kcal mol^{-1}; and third: short-range B and N bonding between 12 to 25 kcal mol^{-1}.

(5) Our work highlights the special utility of derivatives of Aza-bora (*n*)-Annulene for the construction of nano-patterns on the graphite sheet which present a highly attractive combination of strong adsorption via (*n*)-Annulene-graphite π–π* and strong intermolecular interactions towards graphite exfoliation.

Table 5. Ring perimeter, para de-localization (PDI) and para linear response indexes PLR of (*n*)-Annulene (*n* = 8, 10, 12, and 14) and its Aza-bora derivatives

Molecule	Ring perimeter, Å	Para delocalization index (PDI)	Para linear response indexes (PLR)
$C_8H_8^{(2-)}$	11.30	0.030	0.13
$C_8H_8^{(0)}$	11.24	0.032	0.086
$B_4N_4H_8^{2-}$	11.56	0.031	0.16
(10)-Annulene	14.07	0.062	0.474
(12)-Annulene	16.9	0.0313	0.223
(14)-Annulene	23.40	0.074	0.110
(14)-B7N7 Annulene	23.98	0.064	0.121

CONFLICT OF INTEREST

The authors declare that they have no conflicts of interest.

REFERENCES

1. R. Willstätter and E. Waser, Ber. Dtsch. Chem. Ges. **44**, 3423 (1911).
2. W. J. I. Fernández, Y. Mo, and P. V. R. Schleyer, J. Chem. Theory Comput. **8**, 1280 (2012).
3. M. Monajjemi and F. Mollaamin, Biointerface Res. Appl. Chem. **11**, 8298 (2021).
4. R. Naor and Z. Luz, J. Chem. Phys. **76**, 5662 (1982).
5. M. Monajjemi, J. Chem. Phys. **425**, 29 (2013).
6. T. Nishinaga, T. Ohmae, and M. Iyoda, Symmetry **2**, 76 (2010).
7. M. Monajjemi, J. Mol. Model. **20**, 2507 (2014).
8. P. G. Wenthold, D. A. Hrovat, and W. T. Borden, Science (Washington, DC, U. S.) **272**, 1456 (1996).
9. A. Schild and B. Paulus, J. Comput Chem. **34**, 1393 (2013).
10. D. A. Hrovat and W. T. Borden, J. Am. Chem. Soc. **114**, 5879 (1992).
11. M. Monajjemi and J. E. Boggs, J. Phys. Chem. A **117**, 1670 (2013).
12. M. Monajjemi, F. Mollaamin, M. R. Gholami, et al., Main Group Met. Chem. **26**, 349 (2003).
13. T. Yoshida, C. Tokizaki, and T. Takayanagi, Chem. Phys. Lett. **634**, 134 (2015).
14. H. M. Gholiha, A. Ghadami, M. Monajjemi, and M. Ehsani, Biointerface Res. Appl. Chem. **11**, 11316 (2021).
15. E. Steiner, P. W. Fowler, and R. W. A. Havenith, J. Phys. Chem. A **106**, 7048 (2002).
16. F. London, J. Phys. Radium **8**, 397 (1937).
17. L. Pauling, J. Chem. Phys. **4**, 673 (1936).
18. J. A. Pople, J. Chem. Phys. **24**, 1111 (1956).

19. P. V. R. Schleyer, C. Maerker, A. Dransfeld, H. Jiao, and N. J. R. Eikema Hommes, J. Am. Chem. Soc. **118**, 6317 (1996).
20. M. J. Allen, V. C. Tung, and R. B. Kaner, Chem. Rev. **110**, 132 (2010).
21. A. A. Balandin, S. Ghosh, W. Z. Bao, et al., Nano Lett. **8**, 902 (2008).
22. C. Lee, X. D. Wei, J. W. Kysar, and J. Hone, Science (Washington, DC, U. S.) **321**, 385 (2008).
23. X. S. Li, W. W. Cai, J. H. An, S. Kim, et al., Science (Washington, DC, U. S.) **324**, 1312 (2009).
24. J. N. Coleman, Adv. Funct. Mater. **19**, 3680 (2009).
25. J. N. Coleman, Acc. Chem. Res. **46**, 14 (2013).
26. P. L. Kian and Q. Bao, J. Mater. Chem. **20**, 2277 (2010).
27. M. Monajjemi, J. Mol. Liq. **230**, 461 (2017).
28. S. D. Bergin, V. Nicolosi, P. V. Streich, et al., Adv. Mater. **20**, 1876 (2008).
29. S. R. Wang, Y. Zhang, N. Abidi, and L. Cabrales, Langmuir **25**, 11078 (2009).
30. E. A. Meyer, R. K. Castellano, and F. Diederich, Angew. Chem. Int. Ed. **115**, 1210 (2003).
31. M. O. Sinnokrot and C. D. Sherril, J. Phys. Chem. A **110**, 10656 (2006).
32. S. E. Wheeler and K. N. Houk, J. Am. Chem. Soc. **130**, 10854 (2008).
33. H. Jalilian and M. Monajjemi, Jpn. J. Appl. Phys. **54**, 085101 (2015).
34. C. Corminboeuf, P. R. Schleyer, and P. Warner, J. Org. Lett. **9**, 3263 (2007).
35. J. I. Aihara and O. Shizuoka, J. Phys. Chem. A **113**, 7945 (2009).
36. U. Haeberlen, *Advances in Magnetic Resonance*, Supplement 1 (Academic, New York, 1976).
37. M. Mehring, *Principles of High Resolution NMR in Solids* (Springer, Berlin, 1983).
38. P. Diehl, F. Fluck, and R. Kosfeld, *NMR Basic Principles and Progress* (Springer, Berlin, 1978), p. 55.
39. R. K. Harris, E. D. Becker, S. M. Cabral de Menezes, et al., Ann. Magn. Reson. **33**, 41 (2008).
40. J. Herzfeld and A. E. Berger, J. Chem. Phys. **73**, 6021 (1980).
41. R. F. W. Bader, *Atoms in Molecules: A Quantum Theory* (Oxford Univ. Press, Oxford, 1990)
42. A. D. Becke and K. E. Edgecombe, J. Chem. Phys. **92**, 5397 (1990).
43. A. Savin, H.-J. Flad, J. Flad, H. Preuss, and H. G. von Schnering, Angew. Chem. Int. Ed. Engl. **31**, 185 (1992).
44. A. D. Becke, J. Mol. Struct.: THEOCHEM **527**, 51 (2000).
45. R. Zacharia, H. Ulbricht, and T. Hertel, Phys. Rev. B **69**, 155406 (2004).
46. Z. Liu, J. Z. Liu, Y. Cheng, et al., Phys. Rev. B **85**, 205418 (2012).
47. L. X. Benedict, N. G. Chopra, M. L. Cohen, et al., Chem. Phys. Lett. **286**, 490 (1998).
48. X. Feng, S. Kwon, J. Y. Park, and M. Salmeron, ACS Nano **7**, 1718 (2013).
49. E. W. Stout and P. Politzer, Theor. Chim. Acta **12**, 379 (1968).
50. E. M. Sarasia, S. Afsharnezhad, B. Honarparvar, et al., Phys. Chem. Liq. **49**, 561 (2011).
51. L. Mahdavian and M. Monajjemi, Microelectron. Eng. **41**, 142 (2010).
52. M. Otadi, Z. Panahishayegh, and M. Monajjemi, Biointerface Res. Appl. Chem. **11**, 12471 (2021).
53. A. A. Frost and B. Musulin, J. Chem. Phys. **21**, 527 (1953).